

Correlating optimal electrode buffer layer thickness with the surface roughness of the active layer in organic phototransistors

Bo Yao^{a,d}, Yanli Li^a, Zhanwei Wen^a, Maoqing Zhou^a, Wenli Lv^a, Xiao Luo^a, Yingquan Peng^{a,b,*}, Wenhao Li^a, Gu Gong^a, Xingyuan Liu^{c,**}

^a Institute of Microelectronics, School of Physical Science and Technology, Lanzhou University, Lanzhou 730000, People's Republic of China

^b Key Laboratory for Magnetism and Magnetic Materials of the Ministry of Education, Lanzhou University, Lanzhou 730000, People's Republic of China

^c State Key Laboratory of Luminescence and Applications, Changchun Institute of Optics, Fine Mechanics and Physics, Chinese Academy of Sciences, Changchun 130033, People's Republic of China

^d Department of Physics, Shaoxing University, Shaoxing 312000, People's Republic of China

ARTICLE INFO

Article history:

Received 15 January 2014

Received in revised form 22 March 2014

Accepted 30 March 2014

Available online 18 April 2014

Keywords:

Buffer layer

Pentacene

Organic phototransistor

Atomic force microscopy

ABSTRACT

Inserting a C60 buffer layer between Au source/drain electrodes and pentacene active layer has been proved to improve the performances of pentacene organic phototransistors (PENT-OPTs) in our previous study. Buffer layer certainly has an optimal thickness with which the modified device can achieve the best performance. Based on the surface morphology analysis of different thickness C60 buffer layer on pentacene film, we further optimized the thickness of C60 buffer layer for best performance of PENT-OPTs and investigated its physical origins. Studies on PENT-OPTs with different pentacene surface morphology realized by different substrate temperatures indicate that the optimal thickness of C60 buffer layer directly related to the surface roughness of pentacene active layer and it is found that the optimized buffer layer thickness increases with the roughness of pentacene layer. Besides, we found that the photogenerated current of OPTs increases with the increasing of gate electric bias and then gradually reach saturation. An approximate analytical expression for gate voltage dependence of the photogenerated current was derived and used to fit the experiment data. An important parameter, saturated photoresponsivity, was introduced for better comparing the performances of OPTs.

© 2014 Elsevier B.V. All rights reserved.

1. Introduction

Organic field-effect transistors (OFETs) are attracting considerable attention due to their potential applications in low cost and flexible organic integrated circuits [1–4]. Compared with photodiodes, organic phototransistor (OPT) as one of the OFETs family have excellent performance in low noise and high sensitivity, and they have been a novel research area in photodetector during the past few years [5–7].

The performance improvement of organic electronic devices through structural optimization has been one of the focuses of the researchers' attention besides organic molecular modification [8]. It has been proved that the performances of OFETs can be improved

by inserted an appropriate buffer layer between source/drain (S/D) electrodes and active layer [2,3,9–12]. We also found that pentacene-OPT (PENT-OPTs)'s field-effect characteristics and photosensitivity properties could be improved by inserting a C60 buffer layer between Au source/drain electrodes and pentacene active layer in our previous work. The performance enhancements of C60-modified device were interpreted by lowering the total hole injection barrier and increasing the photo-exciton dissociation efficiency [13]. Just like the optimization of OFETs' channel layer thickness [14], theoretically, the performances of the modified devices can be further optimized by adjusting the C60 buffer layer thickness. We supposed that the surface roughness of the active layer may affect the growth of C60 films and further affect the modifying effects of buffer layer in modified devices. It has been shown that the surface morphology of film increases with the increasing of the substrate temperate during film deposited [15,16]. In other words, films with different surface roughness can be realized by deposited at different substrate temperate. Thus, in this study, we especially prepared two series samples of pentacene films deposited at two different substrate temperate ($T_{S,PENT}$)

* Corresponding author at: Institute of Microelectronics, School of Physical Science and Technology, Lanzhou University, Lanzhou 730000, People's Republic of China. Tel.: +86 931 8915362; fax: +86 931 8915362.

** Corresponding author. Tel.: +86 159 4800 5973.

E-mail addresses: yqpeng@lzu.edu.cn (Y. Peng), liuxy@ciomp.ac.cn (X. Liu).

on the OTS (octadecyltrichlorosilane) – treat Si/SiO₂ substrate and used these sample to fabricate C60-modified devices with different thickness C60 buffer layer. The optimal C60 buffer layer thickness was obtained for each series of devices by comparing photosensitivity characteristics of modified-OPTs. We also demonstrated the relationships between the optimal electrode buffer layer thickness and the roughness of the active layer by atomic force microscopy (AFM).

Additionally, we further investigated on the optimal C60-modified device and found that the photogenerated currents (I_{ph}) of OPTs will increase with the increasing of gate electric bias and then gradually reach saturation. An approximate analytical expression for gate voltage (V_{gs}) dependence of I_{ph} was derived and used to fit the experiment data of the optimal device. At last, based on the analysis of the relationship between I_{ph} of OPTs and gate voltage, we introduced an important parameter, saturated photoresponsivity, which can be used for better comparing the performances of OPTs.

2. Experimental

The details of sample growth and the structure of PENT-OPTs modified with C60 buffer layer were described in our previous report [13]. Unlike the previous report, a longer channel length $\sim 50 \mu\text{m}$ was chosen. Two series of PENT-OPTs at $T_{S,PENT}$ of 65 °C and 110 °C were fabricated, respectively, each has five samples with different C60 buffer layer thicknesses (5 nm, 10 nm, 20 nm, 30 nm, 40 nm). For the purpose of surface morphology analysis, samples with the structure of SiO₂/OTS/pentacene and SiO₂/OTS/pentacene/C60 were simultaneously completed during device fabrication. The field-effect characteristics and photoresponsivity were obtained under the same conditions as the previous experiment. AFM analysis was carried out in tapping mode using an Agilent 5500 AFM system.

3. Results and discussion

The photogenerated current (I_{ph}) of OPTs is defined as the drain current difference between under light illumination (I_{ill}) and in the dark (I_{dark}) at the same gate and drain voltage. The dependence of I_{ph} on the C60 buffer layer thickness (d_{buffer}) of PENT-OPTs ($T_{S,PENT} = 65^\circ\text{C}$) at $V_{gs} = 0\text{ V}$ and -100 V are shown in Fig. 1a. It is obvious that the photosensitive characteristic of 20 nm-C60 modified device is superior over the other devices. It obtains 340 nA photogenerated current while PENT-OPT and other modified devices obtains less than 50 nA at zero gate voltage and light intensity (P_{opt}) of 25.74 mW/cm². Similarly, the 20 nm-C60 modified device obtains I_{ph} of 4.83 μA at $V_{gs} = -100\text{ V}$, drain voltage (V_{ds}) of -50 V , which is apparently higher than that of the others. The relationship between I_{dark} and d_{buffer} at $V_{gs} = 0\text{ V}$ and -100 V are shown in Fig. 1b, which is in accordance with the relationship between I_{ph} and d_{buffer} . Both I_{dark} and I_{ph} increase gradually when d_{buffer} is less than 20 nm. After I_{dark} reaching the peak value of 13.54 μA at $V_{gs} = -100\text{ V}$ ($d_{buffer} = 20\text{ nm}$), Both I_{dark} and I_{ph} decrease, even less than that of PENT-OPT without buffer layers. These results indicated that PENT-OPTs ($T_{S,PENT} = 65^\circ\text{C}$) with around 20 nm C60 buffer layer could obtain the best photosensitive characteristics.

As reported in the previous study [13], a thin C60 buffer layer inserted between gold S/D electrodes and pentacene layer could decrease the size of the interface dipole and reduce the hole-injection barrier; moreover, the heterojunction made of pentacene/C60 could effectively enhance the exciton-dissociation efficiency and hence increase I_{ph} . However, holes transfer in C60 layer is limited by the extremely weak hole-transport ability of C60; and a relatively high energy barrier for hole between Au and C60 further decreases the channel currents. We assumed that

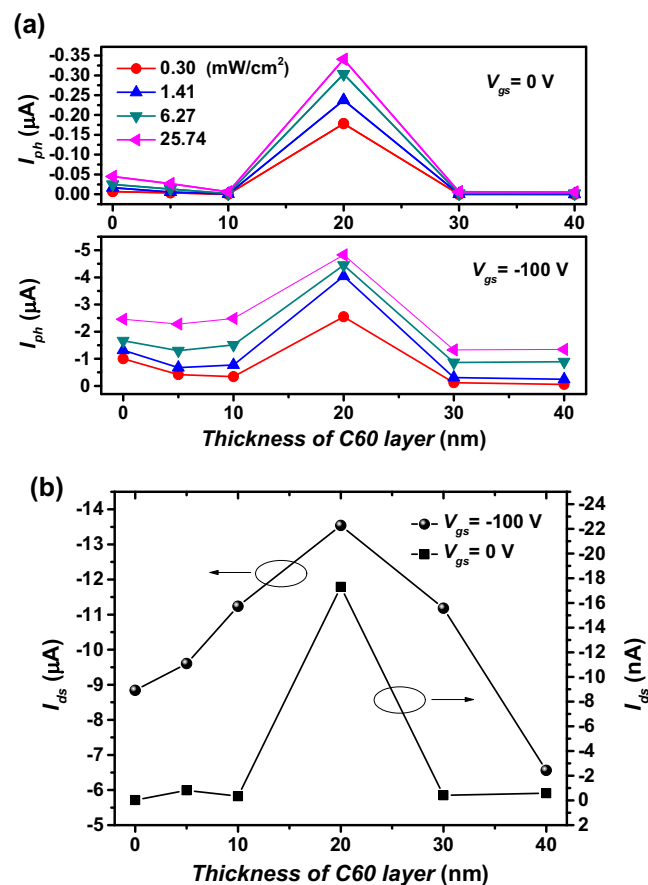


Fig. 1. (a) Plots of I_{ph} as a function of C60 layer thickness at $V_{ds} = -50\text{ V}$ under different light intensities. (b) Plots of I_{dark} as a function of C60 layer thickness at $V_{ds} = -50\text{ V}$.

holes transportation is mainly through direct tunneling in Au-C60-pentacene structure which is in accordance with Park et al. [12] and Sun et al. [3]'s study on the similar OFET structures. The probability of tunneling injection is subject to the tunneling layer thickness, which may be one of the reasons why most of the modified devices' buffer layer are relatively thin, around 0.1–10 nm [2,3,10,12]. However, it can be inferred that the tunneling injection is strongly hindered when d_{buffer} exceeds 20 nm, for C60-modified devices in our study. In other words, the negative effects of 30–40 nm-C60 layer on tunneling injection become more significant than the positive effects of C60 electrode buffer layer: the reduction of the interface dipole and the enhancement of the exciton dissociation efficiency. So 30 & 40 nm-C60 modified devices exhibited poorer performances than the devices with 5–20 nm buffer layer, and even worse than PENT-OPT without buffer layers. Obviously, compared with most of the modified devices' buffer-layer thickness, 20 nm-C60 layer is still relatively thick. To explain why most of the excellent results appeared in the devices with such a buffer layer thickness, we further investigated the surface properties of pentacene and C60 thin-film by atomic force microscope (AFM).

AFM 2D images of 50 nm-pentacene thin film deposited on OTS-treat Si/SiO₂ are shown in Fig. 2. It can be seen that the pentacene grain size is around 200 nm, in agreement with previous observations [1,16]. In the case of pentacene deposited on OTS-treat Si/SiO₂ by conventional vacuum thermal evaporation, the average roughness of the prepared film surface was relatively larger and the root-mean-square (RMS) range of which was about 6–8 nm according to the different evaporation rates [4,17]. The maximum difference in height (peak-to-valley) obtained from inset of Fig. 2

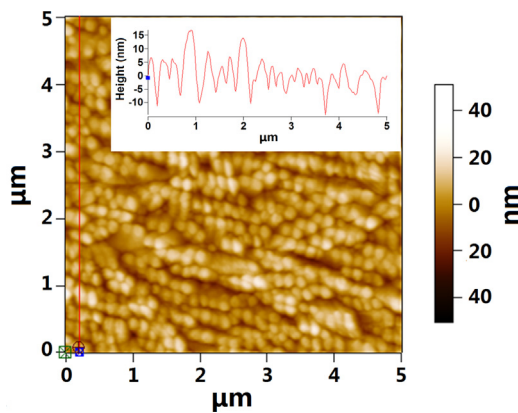


Fig. 2. AFM 2D image of 50 nm-pentacene film on OTS-treat Si/SiO₂; Inset shows the cross-section curve indicated by the red line. (For interpretation of the references to color in this figure legend, the reader is referred to the web version of this article.)

is about 30 nm which indicated that only thick enough C60 buffer layer can fully cover the rough surface of pentacene.

AFM 3D images of pentacene film deposited on OTS-treat Si/SiO₂ and C60 films with five different thicknesses deposited onto the pentacene film are shown in Fig. 3. Obviously, 5 nm-C60 layer was not thick enough to cover pentacene film as shown in Fig. 3b and partially increased the peak height of the film surface. We assume that the surface free energy (SFE) of the pentacene grain shoulder is

lower than that of the grain boundary (valley). Thus, the growth rate of C60 on the shoulder of large pentacene grains may faster than that on the valley of the pentacene film surface at the initial stage of C60 growth, which led to an increase of the film RMS roughness from 7.159 nm to 8.358 nm. Similarly, 10 nm-C60 layer could also not fully cover pentacene film, which led to the RMS roughness of film further increasing to 8.984 nm. Until pentacene film covered by 20 nm-C60 layer, the film surface apparently became smooth and the film RMS roughness decreased to 8.194 nm. As shown in Fig. 3d, only a few of pentacene crystals with large grain size can be seen (marked with red circle in Fig. 3d). We assumed that the SFE of film has been changed when C60 grains partially covering the pentacene films. The SFE on the area of the pentacene grain shoulder covered by C60 is higher than that on the valley of film surface, which lead C60 grains more inclined to grow in the pentacene grain boundary. Thus, the surface RMS of films gradually decreases with the increasing of C60 layer thickness, as shown in Fig. 3d–f. Certainly, the effects of the interface dipole reduction and the exciton dissociation enhancement only appears in the region of pentacene covered by C60 film. However, too thick C60 buffer layer is in fact equivalent to a hole-blocking layer. The probability of carrier tunneling will be reduced when the blocking layer becomes thick. This explains why I_{dark} and I_{ph} under different light intensities firstly increased and then decreased with the increasing of C60-layer thickness.

To further illustrate the relationships between the buffer layer thickness optimization and pentacene surface morphology, we have investigated PENT-OPT and other modified devices at

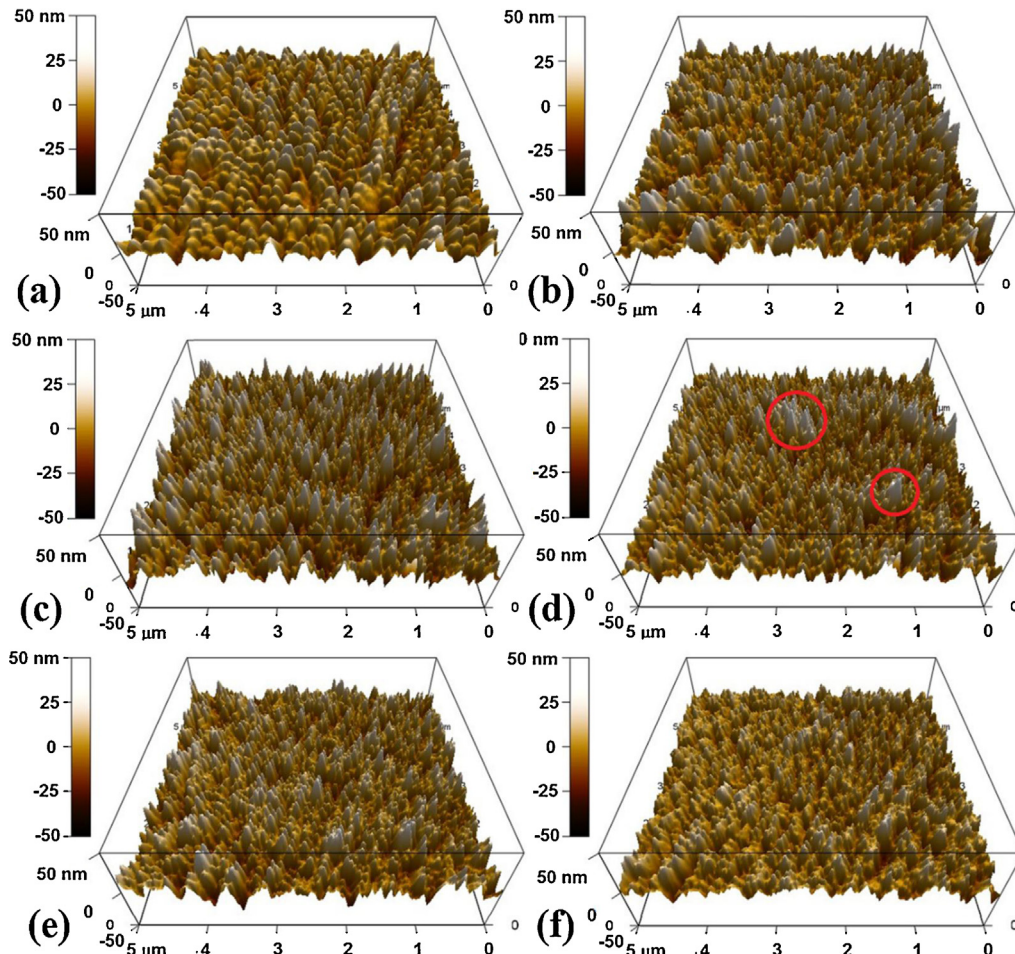


Fig. 3. AFM 3D results of (a) 50 nm-pentacene film on OTS-treat Si/SiO₂, RMS = 7.159 nm and five different thicknesses C60 films deposited onto the pentacene layer. (b) 5 nm, RMS = 8.358 nm; (c) 10 nm, RMS = 8.984 nm; (d) 20 nm, RMS = 8.194 nm; (e) 30 nm, RMS = 7.629 nm; (f) 40 nm, RMS = 6.386 nm.

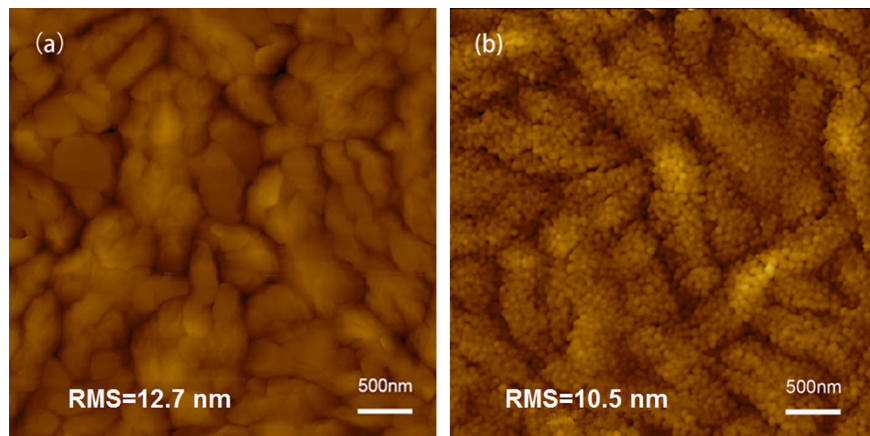


Fig. 4. AFM 2D images of (a) 50 nm-pentacene film on OTS-treat Si/SiO₂ at $T_{S,PENT} = 110^\circ\text{C}$; (b) 30 nm-C60 film deposited on the pentacene layer ($T_{S,PENT} = 110^\circ\text{C}$).

$T_{S,PENT} = 110^\circ\text{C}$ (other conditions remaining the same). The pentacene grain size and surface RMS roughness became larger with increasing substrate temperature in the previous research [15,16]. Thus, the film surface RMS roughness of pentacene at $T_{S,PENT} = 110^\circ\text{C}$ (RMS = 12.70 nm) was larger than that at $T_{S,PENT} = 65^\circ\text{C}$ (RMS = 7.16 nm) while the pentacene grain size of $T_{S,PENT} = 110^\circ\text{C}$ was apparently larger than that of $T_{S,PENT} = 65^\circ\text{C}$, as shown in Figs. 2 and 4a. The surface morphology of 30 nm-C60 film deposited on 50 nm-pentacene film at $T_{S,PENT} = 110^\circ\text{C}$ are shown in Fig. 4b. It can be seen that large-size pentacene grains are fully covered by small C60 grains, forming a continuous film, decreasing the surface RMS roughness from 12.7 nm to 10.5 nm. It means that 30 nm-C60 layer can entirely block the direct contact between Au and pentacene, and effectively decrease the interface dipole.

Fig. 5a and b are the dependences of I_{ph} on C60-buffer-layer thickness, for substrate temperature of $T_{S,PENT} = 110^\circ\text{C}$ and 65°C , respectively. Obviously, the optimal thickness of C60 layer with $T_{S,PENT} = 110^\circ\text{C}$ is around 30 nm, and the optimal C60-layer thickness with $T_{S,PENT} = 65^\circ\text{C}$ is around 20 nm. It can be deduced that the optimal C60-buffer-layer thickness and the pentacene surface morphology are closely-related. The RMS roughness of pentacene film prepared at 110°C is larger than that at 65°C . Thus, a thicker C60 layer is needed to fully cover rougher pentacene film surface at a higher substrate temperature. When the C60 layer thickness

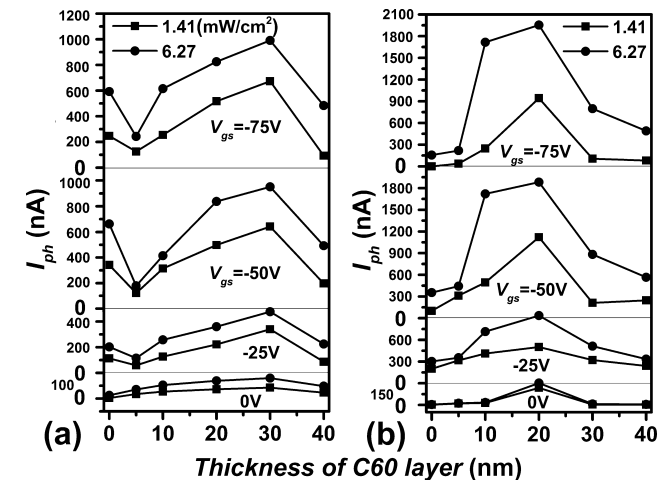


Fig. 5. I_{ph} as a function of C60-layer thickness at different V_{gs} (from 0 to 75 V), $V_{ds} = -50\text{ V}$ and light intensities fixed at 1.41 and 6.27 mW/cm² (a) $T_{S,PENT} = 110^\circ\text{C}$, (b) $T_{S,PENT} = 65^\circ\text{C}$.

is increased beyond the optimal thickness, the carriers tunneling probability will be apparently decreased. As shown in Fig. 5a, I_{ph} of 40 nm-C60 modified device were lower than that of PENT-OPT and others modified device. Compared with the devices prepared at $T_{S,PENT} = 65^\circ\text{C}$, the I_{ph} of devices prepared at $T_{S,PENT} = 110^\circ\text{C}$ were decreased by almost one-half due to the increasing height of grain-boundary potential barriers. Kim et al. in their study reported that higher $T_{S,PENT}$ resulting in much larger and deeper grain boundaries compared with pentacene films grown at low $T_{S,PENT}$ and leading to inferior charge transport properties [18].

The above analysis indicates that the optimal thickness of C60 buffer layer is directly related to the surface roughness of pentacene active layer and the optimized electrode buffer layer thickness increases with increasing the active layer roughness.

Further investigations on PENT-OPT and other modified devices prepared with $T_{S,PENT} = 110^\circ\text{C}$, we found that I_{ph} increased with increasing the gate voltage and eventually reached saturation, as shown in Fig. 6. It means that photoresponsivity (R) which is an important parameter for OPTs may also reach saturation when OPT works with a high enough gate voltage. Among the many research on OPTs, R is usually obtained at gate voltage (V_{gs}) of 0 V or an arbitrary gate voltage [14,19–22]. Actually, most of OPTs are not turning on (working in the OFF-state) with zero gate bias, R obtained in which may not well reveal the real performances of OPTs in the ON-state. And R is strongly dependent on the gate voltage. Therefore, it is difficult to compare the performances of OPTs via R obtained at different V_{gs} in the previous reports of OPTs.

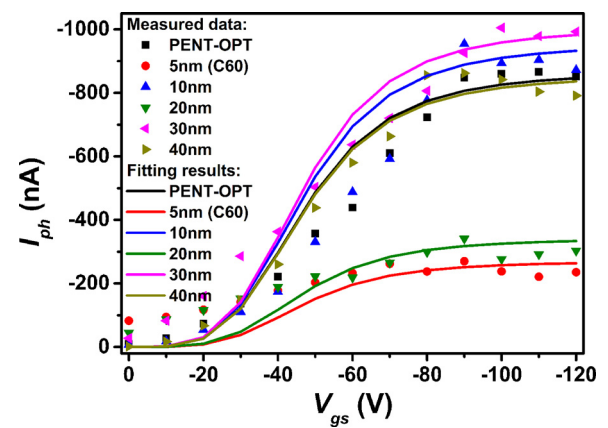


Fig. 6. I_{ph} as a function of gate voltage, symbols and lines represent the measured and the fitting results, respectively.

Table 1

Performance of the devices at $V_{ds} = -50$ V and illumination intensity of 6.27 mW/cm^2 .

	Pent-OPT	Thickness of C60 layer (nm)				
		5	10	20	30	40
V_{gs} (V)	-90	-70	-80	-90	-100	-90
$I_{ph,Max}$ (nA)	-865.848	-269.828	-862.044	-954.128	-1004.994	-340.992
R_{sat} (mA/W)	92	28.68	91.66	101.44	106.86	36.26

It can be indicated from Eq. (1) that R is mainly affected by the incident light power and the photogenerated current.

$$\text{Photoresponsivity } (R) = \frac{I_{ph}}{P_{inc}} = \frac{I_{ill} - I_{dark}}{P_{opt}A}, \quad (1)$$

where P_{opt} is the power of the incident light per unit area, and A is the effective device area ($L \times W$). Larger photogenerated current means higher photoresponsivity when the incident light power and wavelength is kept constant. The photogenerated currents are mainly generated by dissociated excitons which produced by absorbed photons in the light-sensitive layer. The dissociation of excitons is mainly dependent on the electric field in the active layer produced by applied gate and drain voltage, especially the former in OPTs. Thus, excitons can be fully dissociated by a strong electric field under high gate voltage, the photogenerated current eventually reaching saturation. According to Eq. (1), it can be regarded as the maximum photoresponsivity under constant illumination when the photogenerated current of devices reach saturation. We named it as saturated photoresponsivity (R_{sat}) of OPTs, and which is significant for evaluating the performances of OPTs.

Table 1 shows the R_{sat} of these PENT-OPTs prepared with $T_{S,PENT} = 110^\circ\text{C}$ under 6.27 mW/cm^2 illumination at 655 nm . These results are in accordance with previous discussion that PENT-OPTs with 20 and 30 nm C60 buffer layer can obtain higher R_{sat} than the others. Obviously, the optimal OPT with 30 nm C60 buffer layer need the highest gate voltage (-100 V) for achieving the highest R_{sat} .

In order to understand the gate voltage dependence of I_{ph} , we derived an analytical expression for the photogenerated current, which can be expressed as:

$$I_{ph} = q \frac{P_{opt}\alpha d}{hv} P(F), \quad (2)$$

where q is the quantum of electric charge, hv is the photon energy, P_{opt}/hv represents the number of incident photons reaching the surface per unit time; α is the light absorption coefficient, d is the thickness of the photosensitive layer, αd represents the number of excitons generated in the photosensitive layer, F is the magnitude of electric field, which can be approximated to $V_{gs}/(d + d_{buffer})$ for $V_{gs} > V_{ds}$, d_{buffer} is the thickness of the buffer layer and $P(F)$ is the probability of excitons dissociation into free carriers which can be expressed as:

$$P(F) = \frac{k_d(F)}{k_d(F) + k_f}, \quad (3)$$

where $k_d(F)$ is an electric-field dependent dissociation rate, k_f is a decay rate constant. Based on Onsager theory, $k_d(F)$ for dissociation of a bound pair can be expressed as [23,24]:

$$k_d(F) = R \frac{3}{4\pi a^3} e^{-E_B/k_B T} \left[1 + b + \frac{b^2}{3} + \frac{b^3}{18} + \frac{b^4}{180} + \dots \right], \quad (4)$$

where E_B is the electron-hole pair binding energy, a is the initial separation of bound e-h pair.

$$b = \frac{q^3 F}{8\pi\varepsilon_0\varepsilon_r k_B^2 T^2}. \quad (5)$$

Table 2
Parameters used in the fitting calculations.

Parameter	Symbol	Numerical value	References
Dielectric constant of pentacene	ε_r	3	[25]
e/h pair distance	a	1.6 nm	[26]
Incident light power per unit area	P_{opt}	6.27 mW/cm^2	
Hole mobility of pentacene	μ	$0.05 \text{ cm}^2/\text{Vs}$	[12]
Wavelength of the incident light	λ	655 nm	
Thickness	d	50 nm	
Light absorption coefficient	α	10^4 cm^{-1}	Calculated from [12]
Binding energy	E_B	0.55 eV	[27]
Decay rate	k_f	$1.0 \times 10^6 \text{ s}^{-1}$	[24]
Intrinsic charge carrier concentration in pentacene	n_i	$3.1 \times 10^{17} \text{ cm}^{-3}$	[28]
Temperature	T	300 K	

For low mobility semiconductors electron–hole recombination is given by Langevin: $R = q\mu(np - ni^2)/\varepsilon_0\varepsilon_r$, where μ is the spatially averaged sum of electron and hole drift mobilities (For p-type organic material, electron mobility can be ignored), n and p are the electron and hole concentration near the source electrode, ni is the intrinsic charge carrier concentration of pentacene.

The fitting between the photogenerated currents of OPTs and Eq. (2) are shown in Fig. 6, the parameters used in the fitting calculations are shown in Table 2. The trends of fitting results are consistent with that of the experimental data. The fitting are more ideal when applied gate voltage is higher than 80 V. The reasons may be caused by source-drain electric field which were not taken into account in Eq. (2) and we ignored it due to the fact that the gate electric field plays the dominant role in the high gate voltage.

It is very suitable for using saturated photoresponsivity as one of essential parameters to evaluate the performance of OPT. Obviously, compared with photoresponsivity at zero gate voltage, the saturated photoresponsivity obtained in the ON-state are more meaningful.

4. Conclusions

In summary, we have investigated the relationships between the optimal electrode buffer layer thickness and the roughness of the active layer in OPTs. The optimal C60 buffer layer thicknesses around 20 nm or 30 nm were also obtained for PENT-OPTs with $T_{S,PENT} = 65^\circ\text{C}$ or 110°C . The physical origins have been explained through AFM analysis that the rough surface of the pentacene film deposited by traditional organic vacuum evaporation method need thick enough buffer layer to prevent the direct contact between gold and pentacene, and then the inserted C60 buffer layer can reduce the interface dipole and enhance the exciton dissociation

efficiency. An important conclusion that the optimized buffer layer thickness increases with the active layer roughness of OPTs was obtained, which might be advantageous for selecting a more appropriate electrode buffer layer for OPTs. Additionally, according to the further study on the gate voltage dependence of the photogenerated current, saturated photoresponsivity – an important parameter for OPTs was introduced for evaluating the performances of OPTs.

Acknowledgements

This work was supported by the National Natural Science Foundation of China Grant No. 10974074 and the Research Fund for the Doctoral Program of Higher Education of China Grant No. 20110211110005.

References

- [1] G.-C. Yuan, Z. Lu, Z. Xu, C. Gong, Q.-L. Song, S.-L. Zhao, F.-J. Zhang, N. Xu, Y. Gan, H.-B. Yang, C.M. Li, *Org. Electron.* 10 (2009) 1388–1395.
- [2] W. Gu, W. Jin, B. Wei, J. Zhang, J. Wang, *Appl. Phys. Lett.* 97 (2010) 243303.
- [3] Q.-J. Sun, Z. Xu, S.-L. Zhao, F.-J. Zhang, L.-Y. Gao, Y.-S. Wang, *Synth. Met.* 160 (2010) 2239–2243.
- [4] J. Cao, F. Hong, F.-F. Xing, W. Gu, X.-A. Guo, H. Zhang, B. Wei, J.-H. Zhang, J. Wang, *Chin. Phys. B* 19 (2010) 037106.
- [5] Y. Peng, W. Lv, B. Yao, G. Fan, D. Chen, P. Gao, M. Zhou, Y. Wang, *Org. Electron.* 14 (2013) 1045–1051.
- [6] D. Chen, B. Yao, G. Fan, W. Lv, P. Gao, M. Zhou, Y. Peng, *Appl. Phys. Lett.* 102 (2013) 163303.
- [7] B. Mukherjee, M. Mukherjee, Y. Choi, S. Pyo, *ACS Appl. Mater. Interfaces* 2 (2010) 1614–1620.
- [8] Y.-Y. Liu, C.-L. Song, W.-J. Zeng, K.-G. Zhou, Z.-F. Shi, C.-B. Ma, F. Yang, H.-L. Zhang, X. Gong, *J. Amer. Chem. Soc.* 132 (2010) 16349–16351.
- [9] C.-W. Chu, S.-H. Li, C.-W. Chen, V. Shrotriya, Y. Yang, *Appl. Phys. Lett.* 87 (2005) 193508.
- [10] X. Yan, J. Wang, H. Wang, H. Wang, D. Yan, *Appl. Phys. Lett.* 89 (2006) 053510.
- [11] R. Abdur, K. Jeong, M.J. Lee, J. Lee, *Org. Electron.* 14 (2013) 1142–1148.
- [12] J. Park, J. Park, N. Kim, H.-J. Lee, M. Yi, *Jap. J. Appl. Phys.* 47 (2008) 5668–5671.
- [13] B. Yao, W. Lv, D. Chen, G. Fan, M. Zhou, Y. Peng, *Appl. Phys. Lett.* 101 (2012) 163301.
- [14] A. El Amrani, B. Lucas, B. Ratier, *Synth. Met.* 161 (2012) 2566–2569.
- [15] R. Ye, M. Baba, Y. Ohishi, K. Mori, K. Suzuki, *Mol. Cryst. Liq. Cryst.* 407 (2003) 147–155.
- [16] M. Shtain, J. Mapel, J.B. Benziger, S.R. Forrest, *Appl. Phys. Lett.* 81 (2002) 268–270.
- [17] T. Itoh, N. Yamauchi, *Appl. Surf. Sci.* 253 (2007) 6196–6202.
- [18] S.H. Kim, M. Jang, H. Yang, C.E. Park, *J. Mat. Chem.* 20 (2010) 5612.
- [19] H. Xu, J. Li, B.H.K. Leung, C.C.Y. Poon, B.S. Ong, Y. Zhang, N. Zhao, *Nanoscale* 5 (2013) 11850.
- [20] S. Nam, J. Seo, S. Park, S. Lee, J. Jeong, H. Lee, H. Kim, Y. Kim, *ACS Appl. Mater. Interfaces* 5 (2013) 1385–1392.
- [21] Z. Ji, L. Shang, C. Lu, L. Wang, J. Guo, H. Wang, D. Li, M. Liu, *IEEE Electron Dev. Lett.* 33 (2012) 1619–1621.
- [22] Y.-Y. Noh, D.-Y. Kim, *Solid-State Electron.* 51 (2007) 1052–1055.
- [23] C.L. Braun, *J. Chem. Phys.* 80 (1984) 4157.
- [24] L.J.A. Koster, E.C.P. Smits, V.D. Mihailescu, P.W.M. Blom, *Phys. Rev. B* 72 (2005) 085205.
- [25] W.L. Kalb, K. Mattenberger, B. Batlogg, *Phys. Rev. B* 78 (2008) 035334.
- [26] S. Jung, Z. Yao, *Appl. Phys. Lett.* 86 (2005) 083505.
- [27] K. Stokbro, S. Smidstrup, arXiv preprint, 2013 arXiv: 1308.0969.[hep-th].
- [28] Y.S. Lee, J.H. Park, J.S. Choi, *Opt. Mat.* 21 (2003) 433–437.